CHIN. PHYS. LETT. Vol. 38, No. 8 (2021) 087502

Magnetic Anisotropy Induced by Orbital Occupation States in $La_{0.67}Sr_{0.33}MnO_3$ Films

Huaixiang Wang(王怀翔)[1,2], Jinghua Song(宋京华)[1,2], Weipeng Wang(王伟鹏)[1], Yuansha Chen(陈沅沙)[1], Xi Shen(沈希)[1*], Yuan Yao(姚湲)[1], Junjie Li(李俊杰)[1], Jirong Sun(孙继荣)[1,2], and Richeng Yu(禹日成)[1,2*]

[1]*Beijing National Laboratory for Condensed Matter Physics, Institute of Physics, Chinese Academy of Sciences, Beijing 100190, China*

[2]*School of Physics Sciences, University of Chinese Academy of Sciences, Beijing 100049, China*

(Received 20 April 2021; accepted 11 June 2021; published online 2 August 2021)

Interface engineering is an effective and feasible method to regulate the magnetic anisotropy of films by altering interfacial states between films. Using the technique of pulsed laser deposition, we prepared $La_{0.67}Sr_{0.33}MnO_3$ (LSMO) and $La_{0.67}Sr_{0.33}MnO_3/SrCoO_{2.5}$ (LSMO/SCO) films on (110)-oriented $La_{0.3}Sr_{0.7}Al_{0.65}Ta_{0.35}O_3$ substrates. By covering the SCO film above the LSMO film, we transformed the easy magnetization axis of LSMO from the [001] axis to the $[1\bar{1}0]$ axis in the film plane. Based on statistical analyses, we find that the corresponding Mn–Mn ionic distances are different in the two types of LSMO films, causing different distortions of Mn–O octahedron in LSMO. In addition, it also induces diverse electronic occupation states in Mn^{3+} ions. The e_g electron of Mn^{3+} occupies $3z^2 - r^2$ and $x^2 - y^2$ orbitals in the LSMO and LSMO/SCO, respectively. We conclude that the electronic spin reorientation leads to the transformation of the easy magnetization axis in the LSMO films.

DOI: 10.1088/0256-307X/38/8/087502

Transition metal oxide (TMO) films, especially the oxides processed by the interface engineering,[1−6] have attracted extensive attention in the past decades owing to their diverse properties, such as interface charge transfer,[7] two-dimensional electron gas,[8] and discrepancy from bulk materials. Among TMOs, manganates exhibit distinctive performances as a result of the novel magnetic and electronic structures induced by the strong correlation between electrons as well as competition among lattice, charge, spin, and orbit degrees of freedom, for instance, metal–insulator transition,[9] colossal magnetoresistance,[10,11] magnetocaloric effects,[12] and magnetoelectric coupling multiferroic effect.[13]

For an epitaxial film, interfaces,[6] strain induced by a mismatch with the substrate,[14] and restriction of dimension[15] may break the delicate balance among different interactions and result in exotic properties. A fundamental property of magnetic materials is magnetic anisotropy (MA). MA plays a crucial role in many physical phenomena, including magnetic skyrmions,[16] the magnetocaloric effect,[17] and the Kondo effect.[18] There are three types of MA existing in magnetic materials. Magnetocrystalline anisotropy, magnetoelastic coupling anisotropy, and shape anisotropy. Magnetocrystalline anisotropy is independent of grain size and shape while shape anisotropy is the dominant form of anisotropy in small-size specimens.[19,20]

$La_{0.67}Sr_{0.33}MnO_3$ (LSMO), as a perovskite-type magnetic material, is a promising candidate for spintronic materials[21−23] because of its room Curie temperature and 100% spin polarization.[9] For epitaxial thin films, different interfacial couplings cause different MA behaviors.[1,24−26] MA in LSMO has been proved to be closely related to the occupation state of Mn 3*d*-orbital electrons.[27] In general, the mismatch of lattice constant at interface distorts the MnO_6 octahedra of LSMO and controls the electronic occupation state of Mn ions. Revealing the mechanism of MA in the LSMO film will enrich the corresponding scientific understanding and pave the way to future material designs and device applications of spintronic materials. In this work, we find that LSMO and $La_{0.67}Sr_{0.33}MnO_3/SrCoO_{2.5}$ (LSMO/SCO) films, which can be epitaxially grown on (110)-oriented $La_{0.3}Sr_{0.7}Al_{0.65}Ta_{0.35}O_3$ (LSAT) substrates, exhibit different MA behaviors. Using an aberration-corrected transmission electron microscope, we analyze the microstructures of the two films at the atomic scale and investigate the reason for causing the different MA.

The LSMO and LSMO/SCO films were grown epitaxially on (110)-oriented LSAT substrates using the

Supported by the National Key Research Program of China (Grant Nos. 2017YFA0206200, 2016YFA0300701, and 2018YFA0208402), the National Natural Science Foundation of China (Grant Nos. 11934017, 11874413, 11574376, and 51972333), the Strategic Priority Research Program of the Chinese Academy of Sciences(Grant No. XDB33030200), and the Youth Innovation Promotion Association of the Chinese Academy of Sciences (Grant No. 2019009).

*Corresponding authors. Email: rcyu@iphy.ac.cn; xshen@iphy.ac.cn

© 2021 Chinese Physical Society and IOP Publishing Ltd

pulsed laser deposition (PLD) method with a KrF excimer laser ($\lambda = 248$ nm).[28] The LSMO layer is deposited at a temperature of 730℃ in an oxygen pressure of 30 Pa accompanying a laser fluence of 1.6 J/cm^2. The SCO layer is deposited at 700℃ in an oxygen pressure of 12 Pa accompanying a laser fluence of 1.1 J/cm^2. The film thickness is determined by the time of deposition. The magnetic measurements were carried out in a quantum design vibrating sample magnetometer superconducting quantum interference device (VSM SQUID). Thin specimens for transmission electron microscopy (TEM) were prepared by mechanical polishing accompanied by Ar ion milling at liquid nitrogen temperature or focused ion beam (Helios 600I, FEI) technique. The selected area electron diffraction (SAED) observations were performed on a transmission electron microscope (CM200, Philips) with a field-emission gun (FEG) at 200 kV. The high-angle annular dark-field (HAADF) images and electron energy loss spectroscopy (EELS) spectra were acquired on a scanning transmission electron microscope (STEM) equipped with double Cs correctors (CEOS) for the condenser lens and objective lens (ARM200F, JEOL) and a cold FEG at 200 kV. Double tile holders were adopted in TEM studies and controlled by a TEM operate system to ensure the zone axis parallel to the electron beam in all TEM experiments.

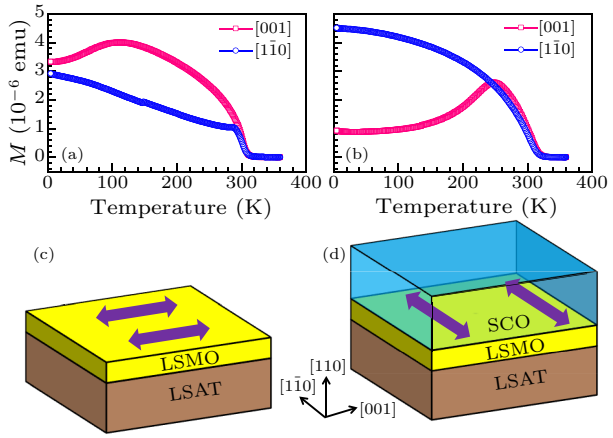

Fig. 1. (a) and (b) Magnetizations as a function of temperature in a field cooling with $H = 100$ Oe corresponding to the LSMO film and LSMO/SCO film grown on LSAT substrates, respectively. Pink and blue curves signify the data obtained from different external magnetic directions. (c) and (d) The schematic diagrams of LSMO film and LSMO/SCO film grown on LSAT substrates. The purple arrows represent the easy magnetization axis of LSMO is along the [001] and [1$\bar{1}$0] axes in the plane of SLF and DLF, respectively.

Two types of films were grown epitaxially on the (110)-oriented LSAT substrates, as schematically shown in Figs. 1(c) and 1(d). Figure 1(c) indicates a single-layered film (SLF) of LSMO with a thickness of 6.5 nm and Fig. 1(d) is double-layered films (DLF) with 6.5 nm LSMO and 35 nm SCO. The magnetizations of the two samples in a field cooling with $H = 100$ Oe as a function of temperature are shown in Figs. 1(a) and 1(b), respectively. The direction of the applied magnetic field is along the [001] and [1$\bar{1}$0] axes, respectively. The corresponding magnetizations are represented by pink and blue curves, respectively. In Figs. 1(a) and 1(b), an obvious increase occurs around 300 K, indicating a ferromagnetic transition. It should be noted that the magnetization along the [001] axis is higher than that along the [1$\bar{1}$0] axis below 280 K in SLF [Fig. 1(a)], however, that is inverse in DLF [Fig. 1(b)]. This means that the easy magnetization axis is along the [001] direction in the SLF whereas along the [1$\bar{1}$0] direction in the DLF.

It is well known that LSAT is a diamagnetic material with a perovskite structure (space group of $Pm\bar{3}m$)[29,30] and SCO has a G-type antiferromagnetic orthorhombic structure with a space group of $Ima2$.[31] Therefore, ferromagnetism only originates from the LSMO film. Meanwhile, there is an extraordinarily strong double exchange interaction between Mn^{3+} and Mn^{4+} ions in the LSMO below T_C.[32] Because of the effect of the crystal field in the LSMO, d-orbitals of Mn ion will split into e_g and t_{2g} orbitals.[33] Moreover, the Jahn–Teller effect[34] degenerates e_g orbitals into x^2-y^2 and $3z^2-r^2$ orbitals. The electronic occupation state of Mn ions is closely related to the crystal structure of LSMO.

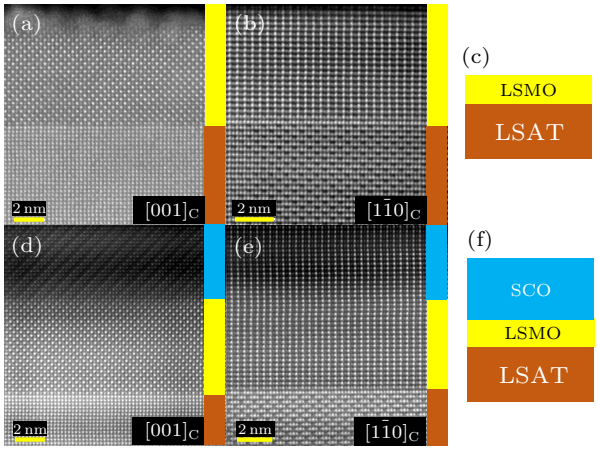

Fig. 2. (a) and (b) The HAADF images of the cross-sectional LSMO SLF along the [001] and [1$\bar{1}$0] axes, respectively. (c) The schematic diagram of SLF. (d) and (e) The HAADF images of the cross-sectional LSMO DLF along the [001] and [1$\bar{1}$0] axes, respectively. (f) The schematic diagram of DLF. (The subscript C in the HAADF images indicates cubic structure.)

In order to explore the microstructures and transformation of the easy magnetization axis in the LSMO film, we carried out TEM observations for the film samples along the cross-section directions at the atomic scale. Figure 2 shows STEM HAADF images of the two samples, indicating the thickness of 6.5 nm for the LSMO and a sharp boundary between

the LSMO and LSAT. A bulk LSMO has a pseudo-cubic structure with $R\bar{3}c$ space group.[35] When it is grown epitaxially on a cubic structure substrate, it will retain the pseudo-cubic structure. Thus, grown on the LSAT, the LSMO film exhibits a perovskite structure, as shown in Figs. 2(a) and 2(b). Since the contrast intensity is approximately proportional to Z^2 (Z is the atomic number) in STEM HAADF images,[36] the brightest spots in the LSMO layer in HAADF images represent La (Sr) atomic columns, and the fainter spots correspond to Mn atomic columns. The O atoms could not be observed in the HAADF images since their scattering is too weak to be acquired at acceptance angles of 90–370 mrad (HAADF). However, there is an indistinct borderline between the LSMO and SCO layers, which instructs a mixed trace of the two components closing to the interface. Moreover, parallel dark stripes occur in the SCO layer and have an angle of 45° relative to the interface, as shown in Fig. 2(d). These dark stripes indicate that the SCO film has a typical brownmillerite structure[37,38] rather than a perovskite structure.

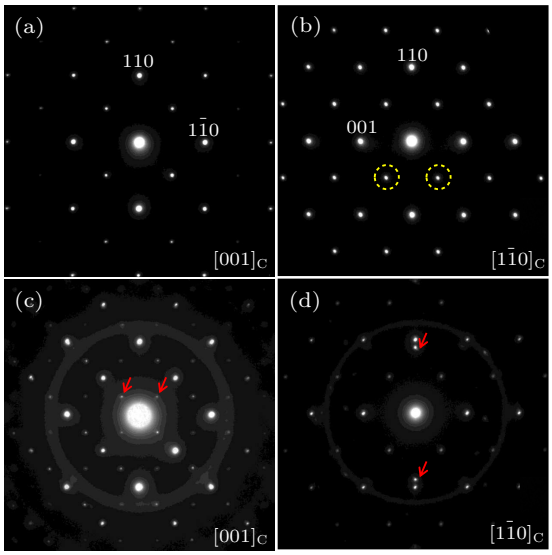

Fig. 3. (a) and (b) Cross-sectional SAED patterns of SLF corresponding to Figs. 2(a) and 2(b). (c) and (d) Cross-sectional patterns of DLF corresponding to Figs. 2(d) and 2(e) (spots marked by red arrows come from the SCO film).

Figures 3(a)–3(d) are the corresponding SAED patterns. All diffraction spots in Figs. 3(a) and 3(b) confirm that the LSMO has the same structure as the LSAT. Compared to Figs. 3(a) and 3(b), Figs. 3(c) and 3(d) show additional spots (marked by red arrows) from the SCO film. In Fig. 3(b), the spots rounded by the yellow dotted circles represent an ordered structure in the LSAT [see Figs. 2(b) and 2(e)]. Al and Ta atoms are locally orderly arranged in B-site of perovskite, which induces a face-centered-cubic structure with a double of the original cell parameters.[39] However, the locally ordered structures would not destroy the perovskite constructions of LSAT and LSMO.

Particularly, in order to research the 45° dark stripes in the SCO layer, the HAADF image closing to the interface between the SCO and LSMO along the [001] zone axis is shown in Fig. 4(a), where the SCO grows to form 90° domains (yellow arrows indicate dark stripes). Such domain structures are also confirmed by the diffraction spots marked by red arrows in Fig. 3(c). Figure 4(b) is a magnified figure of the dotted line rectangle part in Fig. 4(a), which matches well with the structural model of SCO in Fig. 4(c). CoO_6 octahedra and CoO_4 tetrahedra arrange alternately along with the $[100]_C$ and $[010]_C$ directions, as shown in Figs. 4(b) and 4(c). The dark stripes in HAADF images are corresponding to the CoO_4 tetrahedra, indicating a larger Sr-Sr atomic distance compared to that of CoO_6 octahedra in bright stripes. In a word, we have deposited high-quality LSMO epitaxial films and characterized LSAT and LSMO with perovskite structures as well as a perovskite-brownmillerite interface between LSMO and SCO in DLF. Thus, we deduce that the perovskite-brownmillerite interface plays a significant role in the MA in LSMO.[2,40]

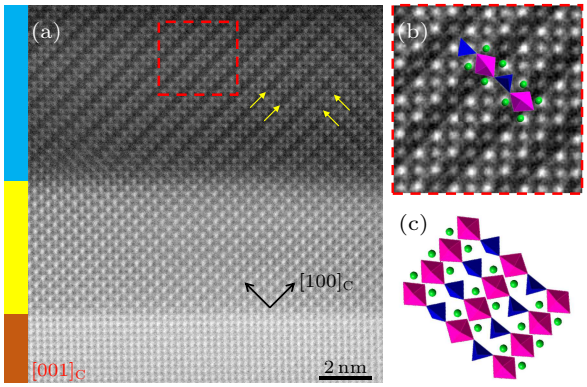

Fig. 4. (a) The HAADF image of cross-sectional LSMO DLF along the [001] zone axis. Yellow arrows indicate dark stripes in the SCO layer. (b) The magnified image of the dotted line rectangle part in (a) and a corresponding structural model overlapped with it. (c) The structural model of SCO (the purple and blue polyhedral represent Co–O octahedra and Co–O tetrahedra, and green balls represent Sr atoms).

Furthermore, in order to quantitatively study the structural difference of LSMO between SLF and DLF, we carried out statistical analyses for the distances of adjacent Mn atoms in corresponding HAADF images. As presented in Fig. 5, we compare the Mn–Mn interatomic distances along the [001], [1$\bar{1}$0] and [110] directions, which are named as $\xi_{[001]}$, $\xi_{[1\bar{1}0]}$ and $\xi_{[110]}$, respectively. The relationship between the distance and Mn–O octahedron is presented in Fig. 5(e). Figures 5(a) and 5(b) show the comparisons between $\xi_{[1\bar{1}0]}$ and $\xi_{[110]}$ averaged from the HAADF image along the

[001] zone axis and between $\xi_{[001]}$ and $\xi_{[110]}$ averaged from the HAADF image along the $[1\bar{1}0]$ zone axis in SLF, respectively. Figures 5(c) and 5(d) show the same comparisons in DLF. Each data point was averaged by dozens of Mn–Mn interatomic distances in corresponding lines. The dotted lines are the averaged values of the corresponding data.

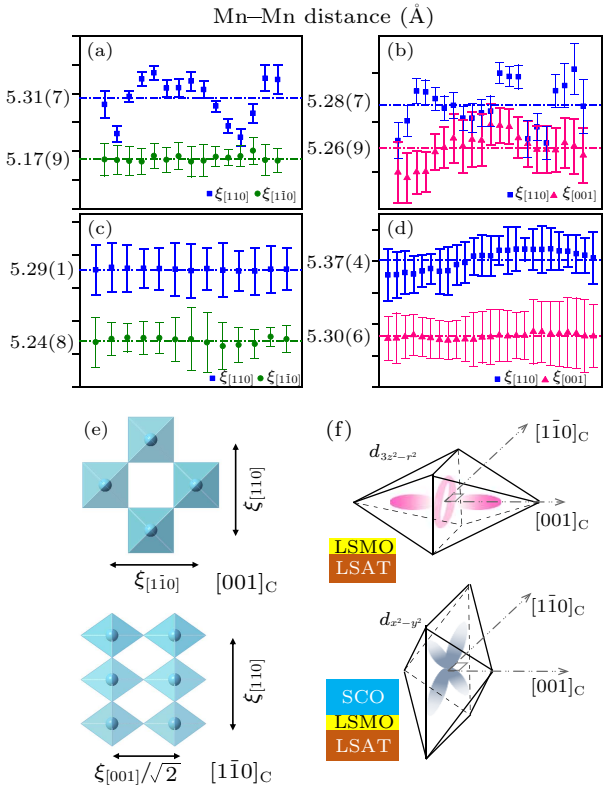

Fig. 5. The statistical interatomic distances of Mn–Mn: (a) $\xi_{[1\bar{1}0]}$ and $\xi_{[110]}$ in SLF obtained from the HAADF image along the $[001]_C$ zone axis; (b) $\xi_{[001]}$ and $\xi_{[110]}$ in SLF obtained from the HAADF image along the $[1\bar{1}0]_C$ zone axis; (c) $\xi_{[1\bar{1}0]}$ and $\xi_{[110]}$ in DLF obtained from the HAADF image along the $[001]_C$ zone axis; (d) $\xi_{[001]}$ and $\xi_{[110]}$ in DLF obtained from the HAADF image along the $[1\bar{1}0]_C$ zone axis. Each data point is averaged by the Mn–Mn distances along a row or a column. The dotted lines are the average values of all corresponding data. (e) Schematic Mn–Mn distances of $\xi_{[001]}$, $\xi_{[1\bar{1}0]}$ and $\xi_{[110]}$ in the structure. (f) The elongated and compressed Mn–O octahedral of LSMO along the $[001]_C$ direction.

Because $\xi_{[001]}$ and $\xi_{[1\bar{1}0]}$ are obtained from different HAADF images, we choose $\xi_{[110]}$ as a reference to compare $\xi_{[001]}$ and $\xi_{[1\bar{1}0]}$.

In SLF:

$\xi_{[1\bar{1}0]}\xi_{[110]} = 97.41\%$,

$\xi_{[001]}\xi_{[110]} = 99.66\%$,

thus, we obtain $\xi_{[001]} > \xi_{[1\bar{1}0]}$.

In DLF:

$\xi_{[1\bar{1}0]}\xi_{[110]} = 99.19\%$,

$\xi_{[001]}\xi_{[110]} = 98.73\%$,

thus, we obtain: $\xi_{[001]} < \xi_{[1\bar{1}0]}$.

As mentioned above, crystal distortion of perovskite degenerates e_g orbitals into x^2-y^2 and $3z^2-r^2$ orbitals. The spin of e_g electron is coupled to the orbital by spin-orbital interaction, and the orbital is affected by the crystal symmetry. According to the Bruno model,[24] though the orbital magnetic moment is exceedingly small, its direction would affect the direction of the easy magnetization axis. The direction of orbital magnetic moment is determined by the occupation state of the e_g electron. According to the previous reports, the pseudo-cubic lattice parameters of bulk SCO, LSMO, and LSAT are 3.915 Å, 3.876 Å and 3.868 Å, respectively.[31,41,42] Hence the LSMO layer suffers from compressive and tensile strain by LSAT and SCO with approximately −0.21% and 1.10%, respectively. Although enduring the equal lattice mismatch along the [001] and $[1\bar{1}0]$ directions in SLF by the cubic structure of LSAT, LSMO film under compressive strain would perform anisotropic distortion of oxygen octahedra.[43,44] For DLF, a completely different state occurs at the interface between LSMO and SCO. The tensile strain is much stronger than that affected by the substrate. In oxide compounds, the deficiency of O content causes lattice expansion.[45] Thus, the oxygen-deficient CoO_4 sub-layer in brownmillerite SCO film leads to the elongation of tetrahedra along [100] or [010] directions in different domains.[46] It also causes the elongation of the MnO_6 octahedra along the superstructural direction of the SCO layer because of the direct connection between MnO_6 octahedra and CoO_4 tetrahedra at the interface, which changes the orbital occupation state of Mn ions. In SLF, $\xi_{[001]} > \xi_{[1\bar{1}0]}$ causes an elongated octahedral along the [001] direction, as shown in Fig. 5(f), and the lower energy of $3z^2 - r^2$ orbital compared to $x^2 - y^2$ orbital. In this case, the e_g electron of Mn^{3+} preferentially occupies $3z^2 - r^2$ orbital. This induces an easy magnetization axis along the [001] direction in SLF. Relatively, in DLF, $\xi_{[001]} < \xi_{[1\bar{1}0]}$ leads to a compressed octahedral along the [001] direction, as shown in Fig. 5(f), and the lower energy of $x^2 - y^2$ orbital, thus, the e_g electron prefers to occupy $x^2 - y^2$ orbital. In the LSMO film plane, the $[1\bar{1}0]$ direction is along the projection of the $x^2 - y^2$ orbital. Thus, the occupation of e_g electron in $x^2 - y^2$ orbital induces an easy magnetization axis along the $[1\bar{1}0]$ direction. This is consistent with the result of x-ray linear dichroism.[28] Our results indicate that the stronger strain produced by the lattice mismatch at the perovskite-brownmillerite interface in the DLF results in a different distortion of MnO_6 octahedra in LSMO from that in the SLF. Different distortions of the octahedral lead to different orbital occupancies of e_g electron of Mn^{3+} ion, which transforms the easy magnetization axis along the [001] direction in SLF to the $[1\bar{1}0]$ direction in DLF in the film plane.

Charge transfer between Mn and Co ions was mentioned to explain the phenomenon of MA in an LSMO

film.[40] In Fig. 6, we present the EELS spectra of the DLF in an energy range from 625 eV to 875 eV. Each spectrum is an integration of the line scan profiles along the [1$\bar{1}$0] direction when the sample was observed along the [001] zone axis. We obtained EELS spectra from the LSMO layer to the SCO layer across the interface as shown in Fig. 6. Obviously, near the interface between LSMO and SCO, both of the Mn and Co peaks appear simultaneously, indicating a mixture of several atomic layers. This is consistent with the blurry borderline in Fig. 2(d) and causes stronger crystal distortions. However, there is no obvious shift of Mn L edge from the LSMO layer to the interface, indicating no change of valence state for Mn ions. In contrast, a shift of the Co L_3 peak toward low energy can be noticed from the Co layer to the interface, suggesting a decrease of valence state for Co ions. This may be due to the fact that $SrCoO_{3-\delta}$ $(0 < \delta < 1)$ exists as an impurity in local areas results from the change of local oxygen content in the SCO film.[28,47] Therefore, there may be no charge transfer between Mn and Co ions in the DLF.

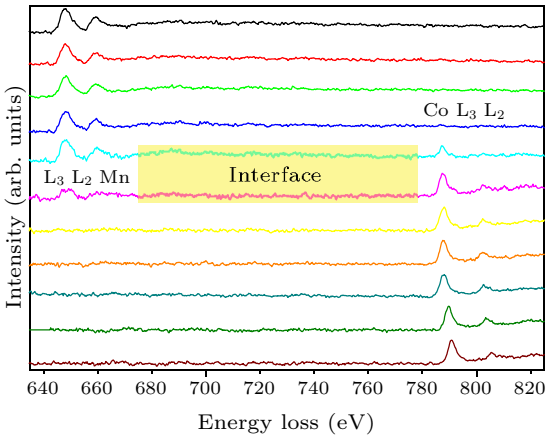

Fig. 6. Integrated EELS spectra from the LSMO layer to the SCO layer (all data was corrected according to the zero-loss peak).

In summary, we have investigated the MA of LSMO films in LSMO and LSMO/SCO films grown epitaxially on (100)-oriented LSAT substrates. Magnetic measurements display an easy magnetization axis of LSMO along the [001] direction in SLF while along the [1$\bar{1}$0] direction in DLF. Through the quantitative statistical analyses, we find that the Mn–O octahedral distortions are different in these two film samples. In SLF, the octahedra are elongated, while in DLF, the octahedra are compressed. This gives rise to the preferential occupation of e_g electron in the $3z^2 - r^2$ orbital of Mn in SLF while in the $x^2 - y^2$ orbital in DLF. Thus, it is concluded that the anomalous MA transformation of LSMO from the [001] direction in SLF to the [1$\bar{1}$0] in DLF originates from a spin orientation of Mn ions. Our EELS spectra reveal that there is no detectable charge transfer between Mn and Co ions.

References

[1] Yi D, Liu J, Hsu S L, Zhang L, Choi Y, Kim J W, Chen Z, Clarkson J D, Serrao C R, Arenholz E, Ryan P J, Xu H, Birgeneau R J and Ramesh R 2016 *Proc. Natl Acad. Sci. USA* **113** 6397
[2] Zhang J, Zhong Z, Guan X, Shen X, Zhang J, Han F, Zhang H, Zhang H, Yan X, Zhang Q, Gu L, Hu F, Yu R, Shen B and Sun J 2018 *Nat. Commun.* **9** 1923
[3] Song J, Chen Y, Zhang H, Han F, Zhang J, Chen X, Huang H, Zhang J, Zhang H, Yan X, Khan T, Qi S, Yang Z, Hu F, Shen B and Sun J 2019 *Phys. Rev. Mater.* **3** 045801
[4] Guan X, Shen X, Zhang J, Wang W, Zhang J, Wang H, Wang W, Yao Y, Li J, Gu C, Sun J and Yu R 2019 *Phys. Rev. B* **100** 014427
[5] Dagotto E 2007 *Science* **318** 1076
[6] Hwang H Y, Iwasa Y, Kawasaki M, Keimer B, Nagaosa N and Tokura Y 2012 *Nat. Mater* **11** 103
[7] Chakhalian J, Freeland J W, Habermeier H U, Cristiani G, Khaliullin G, van Veenendaal M and Keimer B 2007 *Science* **318** 1114
[8] Ohtomo A and Hwang H Y 2004 *Nature* **427** 423
[9] Park J H, Vescovo E, Kim H J, Kwon C, Ramesh R and Venkatesan T 1998 *Nature* **392** 794
[10] Jin S, Tiefel T H, McCormack M, Fastnacht R A, Ramesh R and Chen L H 1994 *Science* **264** 413
[11] von Helmolt R, Wecker J, Holzapfel B, Schultz L and Samwer K 1993 *Phys. Rev. Lett.* **71** 2331
[12] Moya X, Hueso L E, Maccherozzi F, Tovstolytkin A I, Podyalovskii D I, Ducati C, Phillips L C, Ghidini M, Hovorka O, Berger A, Vickers M E, Defay E, Dhesi S S and Mathur N D 2013 *Nat. Mater* **12** 52
[13] Kimura T, Goto T, Shintani H, Ishizaka K, Arima T and Tokura Y 2003 *Nature* **426** 55
[14] Cao J and Wu J 2011 *Mater. Sci. Eng. R* **71** 35
[15] Boris A V, Matiks Y, Benckiser E, Frano A, Popovich P, Hinkov V, Wochner P, Castro-Colin M, Detemple E, Malik V K, Bernhard C, Prokscha T, Suter A, Salman Z, Morenzoni E, Cristiani G, Habermeier H U and Keimer B 2011 *Science* **332** 937
[16] Rößler U K, Bogdanov A N and Pfleiderer C 2006 *Nature* **442** 797
[17] Reis M S, Rubinger R M, Sobolev N A, Valente M A, Yamada K, Sato K, Todate Y, Bouravleuv A, von Ranke P J and Gama S 2008 *Phys. Rev. B* **77** 104439
[18] Otte A F, Ternes M, von Bergmann K, Loth S, Brune H, Lutz C P, Hirjibehedin C F and Heinrich A J 2008 *Nat. Phys.* **4** 847
[19] Poulopoulos P and Baberschke K 1999 *J. Phys.: Condens. Matter* **11** 9495
[20] Allenspach R 1994 *J. Magn. Magn. Mater.* **129** 160
[21] Fert A, Barthélémy A, Youssef J B, Contour J P, Cros V, De Teresa J M, Hamzic A, George J M, Faini G, Grollier J, Jaffrès H, Le G H, Montaigne F, Pailloux F and Petroff F 2001 *Mater. Sci. Eng. B* **84** 1
[22] Garcia V, Bibes M, Bocher L, Valencia S, Kronast F, Crassous A, Moya X, Enouz-Vedrenne S, Gloter A, Imhoff D, Deranlot C, Mathur N D, Fusil S, Bouzehouane K and Barthelemy A 2010 *Science* **327** 1106
[23] Pantel D, Goetze S, Hesse D and Alexe M 2012 *Nat. Mater* **11** 289
[24] Zhang J, Yan X, Han F, Zhang J, Liu D, Shen B and Sun J 2018 *AIP Adv.* **8** 055809
[25] Okada Y, Walkup D, Lin H, Dhital C, Chang T R, Khadka S, Zhou W, Jeng H T, Paranjape M, Bansil A, Wang Z, Wilson S D and Madhavan V 2013 *Nat. Mater.* **12** 707
[26] Majumdar S, Kooser K, Elovaara T, Huhtinen H, Granroth

S and Paturi P 2013 *J. Phys.: Condens. Matter* **25** 376003
[27] Bruno P 1989 *Phys. Rev. B* **39** 865
[28] Song J, Chen Y, Chen X, Wang H, Khan T, Han F, Zhang J, Huang H, Zhang J, Zhang H, Zhang H, Yan X, Qi S, Hu F, Shen B, Yu R and Sun J 2019 *Phys. Rev. Appl.* **12** 054016
[29] Khalid M, Setzer A, Ziese M, Esquinazi P, Spemann D, Pöppl A and Goering E 2010 *Phys. Rev. B* **81** 214414
[30] Wang D Y, Wang J, Chan H L W and Choy C L 2007 *J. Appl. Phys.* **101** 043515
[31] Muñoz A, de la C C, Alonso J A, Botta P M, Pardo V, Baldomir D and Rivas J 2008 *Phys. Rev. B* **78** 054404
[32] Anderson P W and Hasegawa H 1955 *Phys. Rev.* **100** 675
[33] Tokura Y 2000 *Science* **288** 462
[34] Jahn H and Teller E 1937 *Proc. R. Soc. Lond. A* **161** 220
[35] Venkataiah G, Krishna D C, Vithal M, Rao S S, Bhat S V, Prasad V, Subramanyam S V and Reddy P V 2005 *Physica B* **357** 370
[36] Jesson D E and Pennycook S J 1995 *Proc. R. Soc. Lond. A* **449** 273
[37] Zhang J, Chen X, Zhang Q, Han F, Zhang J, Zhang H, Zhang H, Huang H, Qi S, Yan X, Gu L, Chen Y, Hu F, Yan S, Liu B, Shen B and Sun J 2018 *ACS Appl. Mater. Interfaces* **10** 40951
[38] Wang W, Zhang J, Shen X, Guan X, Yao Y, Li J, Gu C, Sun J, Zhu Y, Tao J and Yu R 2020 *Phys. Rev. B* **101** 024406
[39] Li H, Salamanca-Riba L, Ramesh R and Scott J H 2003 *J. Mater. Res.* **18** 1698
[40] Cui B, Li F, Song C, Peng J J, Saleem M S, Gu Y D, Li S N, Wang K L and Pan F 2016 *Phys. Rev. B* **94** 134403
[41] Martin M C, Shirane G, Endoh Y, Hirota K, Moritomo Y and Tokura Y 1996 *Phys. Rev. B* **53** 14285
[42] Chakoumakos B C, Schlom D G, Urbanik M and Luine J 1998 *J. Appl. Phys.* **83** 1979
[43] Boschker H, Mathews M, Brinks P, Houwman E, Vailionis A, Koster G, Blank D H A and Rijnders G 2011 *J. Magn. Magn. Mater.* **323** 2632
[44] Vailionis A, Boschker H, Houwman E, Koster G, Rijnders G and Blank D H A 2009 *Appl. Phys. Lett.* **95** 152508
[45] Adler S B 2004 *J. Am. Ceram. Soc.* **84** 2117
[46] Jeen H, Choi W S, Biegalski M D, Folkman C M, Tung I C, Fong D D, Freeland J W, Shin D, Ohta H, Chisholm M F and Lee H N 2013 *Nat. Mater* **12** 1057
[47] Zhang Q, He X, Shi J, Lu N, Li H, Yu Q, Zhang Z, Chen L Q, Morris B, Xu Q, Yu P, Gu L, Jin K and Nan C W 2017 *Nat. Commun.* **8** 104